*AAPS PharmSciTech, Vol. 12, No. 4, December 2011 (© 2011)*
DOI: 10.1208/s12249-011-9688-9

*Research Article*

# Anti-Osteoporotic Drug Release from Ordered Mesoporous Bioceramics: Experiments and Modeling

**Miguel Manzano,[1,2] Gaetano Lamberti,[3] Ivan Galdi,[3] and María Vallet-Regí[1,2,4]**

*Received 21 June 2011; accepted 2 September 2011; published online 16 September 2011*

***Abstract.*** The release of a potent bone-resorption inhibitor such as zoledronate from a versatile drug delivery system such as SBA 15 has been modeled. The initial and boundary conditions have been defined, together with the system parameters, including the determination of equilibrium and transport parameters. Additionally, the experimental model of the same system has been observed to validate the prediction here developed. This approach represents a powerful tool for the designing of mesoporous implantable drug delivery systems because their release kinetics can be predicted in advance, and this leads to a considerable time and resources saving.

**KEY WORDS:** drug delivery; modeling; ordered mesoporous matrices.

## INTRODUCTION

Drug delivery systems are nowadays one of the most promising fields in biotechnology. They are based on the process of administering a pharmaceutical product to achieve the desired therapeutic effect. The goal of drug delivery systems is to maintain the concentration of drugs in the precise sites of the body within the optimal dosage and below the toxicity levels to improve the therapeutic efficacy and reduce toxicity (1). There are several organic materials that have been employed as drug delivery vectors, such as polymeric nanoparticles, liposomes, and micelles, and other inorganic materials with better chemical and mechanical stability that are nontoxic and biocompatible, such as certain porous silica materials. In addition, these delivery vectors are of particular interest when unstable or very poorly soluble drugs need to be employed.

An important advance on this type of technology has arisen with the development of targeted delivery systems to direct the drugs where they are specifically needed. In fact, a great effort is currently being devoted in biomedicine to deliver the pharmaceutical compounds to the patient through the use of the most appropriated route from the physiological point of view. In conventional medicine, the most common routes for taking drugs are oral administration, injection, and transdermal treatments. However, depending on the therapy, these methods might present a lack of efficiency, as it happens to occur in the case of bone tissue pathologies where the area is poorly irrigated. In those cases, for the treatment of bone tissue, implantable drug delivery systems for local drug release should be employed. In those cases, the employed materials should perform the desired biological response when dealing with the physiological environment together with the ability of releasing the desired payload of drugs. Regarding these tasks, nanostructured mesoporous silica materials have been shown to fulfill both of them: they can regenerate osseous tissue (2,3) and they are able to act as controlled release systems (4).

The unique properties of ordered mesoporous materials have promoted their employment on biomedical applications as implantable drug delivery bioceramics (5,6). Their high surface area (~1,000 $cm^2/g$) assures a high potential for drug adsorption. Their high pore volume (~1 $cm^3/g$) allows the hosting of a great amount of biomolecules into their mesostructure of cavities. Their well-ordered mesopore distribution guarantees homogeneity and reproducibility on drug adsorption and release processes. The feasible functionalization of their walls, which present a high density of silanol groups, allows to design matrices to improve the adsorption capacity or retard the release kinetics of the adsorbed biomolecules. In addition to all of this, their chemical composition, similar to bioglasses (7), makes them appropriate materials to be employed in osseous regeneration technologies (8).

In the treatment of bone tissue pathologies, especially on those osteoarticular disorders associated with increase bone resorption such as osteoporosis, Paget's disease, and osteolytic tumors, bisphosphonates like zoledronate (Fig. 1) are currently being employed (9). However, these pharmaceutical agents present low intestinal adsorption when orally administrated (10), with an intestinal adsorption of less than 1%. Therefore, high doses of these drugs are needed to reach the action areas which provoke gastrointestinal disturbances (11), chronic renal failures, and osteonecrosis of the jaws (12). An alternative for this treatment is employing implantable drug

[1] Department of Inorganic and Bioinorganic Chemistry of the Faculty of Pharmacy, Universidad Complutense de Madrid, Madrid 28040, Spain.
[2] Biomedical Research Networking Center in Bioengineering, Biomaterials and Nanomedicine, CIBER-BBN, Barcelona, Spain.
[3] Department of Industrial Engineering, University of Salerno, Via Ponte don Melillo, 84084 Fisciano, Salerno, Italy.
[4] To whom correspondence should be addressed. (e-mail: vallet@farm.ucm.es)

 

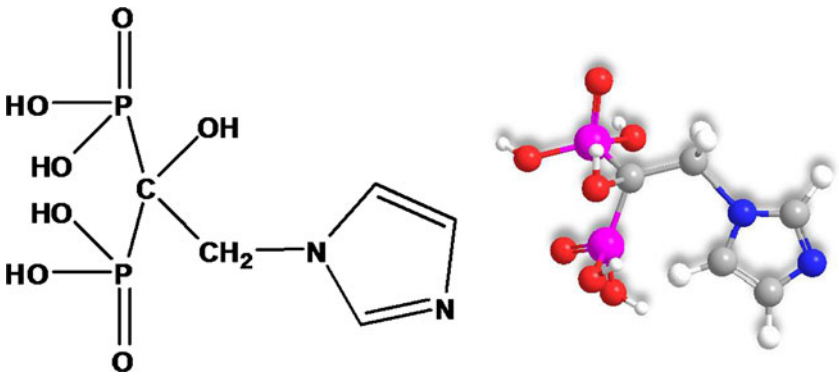


**Fig. 1.** Chemical structure of zoledronate (diameter of ca. 1 nm), a bisphosphonate employed in the treatment of certain bone tissue diseases

delivery vectors to release the pharmaceutical agent exactly in the place where it is specifically needed. This technology has been explored using polymeric microspheres (13,14), organic–inorganic composites (15), and calcium phosphates (16,17). It is also possible to employ the abovementioned ordered mesoporous ceramics to exploit all the advantages that these systems present over traditional systems (18–21).

In all drug delivery systems, as in the whole pharmacotherapy, the development of systems capable of predetermine the release profile of a drug is an important tool (22). In the present work, the release of zoledronate from SBA 15 materials has been modeled; to verify this prediction, SBA 15 materials have been loaded with the same bisphosphonate and release experiments have been carried out aiming to validate the model here proposed with experimental data.

## EXPERIMENTAL

### Materials

Tetraethyl orthosilicate (TEOS, Aldrich) was used as received. Reagent-grade hydrochloric acid (HCl, 37%, Panreac), sodium hydroxide (NaOH, 98%, Panreac), sodium chloride (NaCl, 98%, Panreac), and tris(hydroxymethyl) aminomethane ($(HOCH_2)_3CNH_2$, 99.9%, Aldrich) were used without further purification. Polyoxyethylene–polyoxypropylene block copolymer ($PEO_{20}$-$PPO_{70}$-$PEO_{20}$, Pluronic® P123) was kindly supplied by BASF Co. (New Jersey, USA). Chromasolv® acetonitrile and water for HPLC (gradient grade) were obtained from Sigma-Aldrich. Zoledronate, (1-hydroxyl-2-imidazol-1-yl-1-phosphonoethyl)phosphonic acid, ($C_5H_{10}N_2O_7P_2$), a potent inhibitor of osteoclastic bone resorption, was kindly provided by Novartis, and it was used without further purification.

### Methods

Ordered mesoporous SBA 15 bioceramics were synthesized following the procedure described by Zhao *et al.* elsewhere (23). The template solution was produced dissolving 4 g of the surfactant Pluronic® P123 in deionized water (104 mL) and 37% HCl (20 mL) under magnetic stirring. Once the surfactant was completely dissolved, TEOS (9.6 mL) was added to the template solution to yield a molar composition of $1.0SiO_2$:0.017P123:6.03HCl:$145H_2O$. This solution was magnetically stirred for 12 h at room temperature in a sealed Teflon container and subsequently aged at 100°C for 24 h. The obtained solid silica particles were then filtered, washed with deionized water, and dried at 60°C for 12 h. To conclude, the obtained powder was thermally treated at 550°C under $N_2$ flow for 2 h and then under atmospheric air for further 2 h, leading to the surfactant removal.

### Material Characterization

Small-angle X-ray diffraction (XRD) was employed to confirm the ordered mesostructure of the produced material. XRD patterns were recorded in a Philips X'Pert diffractometer equipped with Cu Kα (40 kV, 20 mA) over the range 0.6–10.0° with a step of 0.02° and an analysis time of 5 s.

The surface characterization of materials was carried out by $N_2$ adsorption/desorption analysis at −196°C using a Micromeritics ASAP2010 analyzer. To perform the test, 50 mg of material was degassed at 60°C for 24 h under a vacuum lower than $10^{-5}$ Torr before the analysis.

The chemical composition of the silica material was confirmed using Fourier-transformed infrared (FTIR) spectroscopy, which was performed with a Nicolet Nexus spectrometer using the KBr pellet method. In addition, the complete surfactant removal was confirmed by elemental analysis, in a PerkinElmer 2400 CHN analyzer, and thermogravimetric analysis, in a dynamic nitrogen atmosphere between 30°C and 950°C (air flow rate of 50 mL $min^{-1}$ with a heating rate of 10°C $min^{-1}$) using a PerkinElmer Pyris Diamond analyzer.

### Zoledronate Loading and Release

Zoledronate adsorption was performed by soaking 800 mg of powered SBA 15 material in 8 mL of an aqueous zoledronate solution (40 mg $mL^{-1}$) buffered at pH 6 for 24 h at 37°C. Then, the loaded materials were centrifuged, rinsed with deionized water, and centrifuged again to remove the non-adsorbed drug molecules. Zoledronate loading was confirmed using FTIR spectroscopy and quantified using X-ray fluorescence (XRF) spectroscopy in a Philips PANanalytical AXIOS spectrometer, in which X-rays were generated using the Rh Kα line at $\lambda$=0.614 Å. After drying the loaded materials, portions of 100 mg of zoledronate-loaded materials were then compacted using uniaxial and isostatic pressures at room temperature to obtain disks with diameters of 13 mm.

The *in vitro* delivery assays were performed by soaking each disk of SBA 15 material in 10 mL of NaCl 0.9% solution at 37°C and physiological pH 7.4. To avoid limitation of the delivering rate by external diffusion constrains, continuous stirring was maintained during the delivery assays. The delivered zoledronate concentration was monitored by reversed-phase high performance liquid chromatography (RP-HPLC) in a Waters Alliance automatic analysis system comprising a Model 2695 separations module and a Model 2996 photodiode array detector. The RP-HPLC procedure for the determination of zoledronate was carried out with a 250× 4.6 mm prepacked analytical column XTerra RP18 (Waters) containing 5-μm C-18 functionalized silica beads. The isocratic mobile phase was a mixture of a 10 nM phosphate aqueous solution and methanol (90:10, *v*/*v*) at 0.7 mL $min^{-1}$ and 25°C. The injection volume was 10 μL, and detection was performed by UV at 210 nm. Under these conditions, the retention time of zoledronate was 3.8 min. Several zoledronate solutions at concentrations of 0, 0.125, 0.25, 0.375, 0.5, 0.625, 0.75, 0.875, and 1 mg $mL^{-1}$ in aqueous NaCl 0.9% buffered at pH 7.4 were used as standards. The calibrated plot showed a good correlation coefficient >0.99. The chromatographic peaks were observed to be stable and at the same retention time during the analysis.

## Modeling

The drug release processes could be described by means of mass balances, on differential volumes, in transient and accounting for transport phenomena and reactions. Mathematically, this means that the phenomena were described by systems of partial differential equations (PDEs). The nonlinearity of the problem, as well as parameter variability and complex shapes which could be involved, asks for numerical solutions. The most effective method to solve sets of PDEs is the class of finite element methods (FEM) (24). The FEM software used in this work to implement the simulations is COMSOL Multiphysics® 3.4 (Copyright © 1994–2007 by COMSOL AB, Tegnérgatan 23 SE-111 40 Stockholm). It is a powerful interactive environment for modeling and solving all kind of scientific and engineering problems based on PDEs; this software allows transforming conventional models for each kind of physical model into multiphysics models, which solve coupled physics phenomena simultaneously (25). The development and implementation of the simulations have been carried out with the help of a workstation based on the processor Intel® Core™2 Duo E8500, with a clock rate of 3.16 GHz and a RAM of 3 GB, 800 MHz.

During the release process of a drug loaded into a porous matrix, the system can be described as a biphasic medium, constituted by the matrix on which the active principle is joined (the bio-ceramic) and a fluid phase (initially solute free) that penetrates porous structure's cavities and dissolves the drug, making it capable to diffuse out to the external medium. Between the two phases, equilibrium and mass transfer phenomena establish, whose modeling can be described through equilibrium relations, mass transfer equations and material balances, implemented with reference to the transferring component (the drug), on differential volumes of the system (the mesoporous bio-ceramic particle). The object of modeling is the determination of both the concentration of the drug immobilized in the solid matrix ($Q$, $mg_{drug}/mg_{matrix}$) (Eq. 1) and the concentration of the drug in the dissolution medium which infiltrates into the pores ($C$, $mg_{drug}/mg_{fluid}$) (Eq. 2).

$$Q = Q\left(t, \vec{x}, \Lambda\right) \tag{1}$$

$$C = C\left(t, \vec{x}, \Lambda\right) \tag{2}$$

Both the concentrations are functions of independent temporal ($t$) and spatial $\left(\vec{x}\right)$ variables and of the system's physical parameters vector ($\Lambda$).

Accounting for the flux from the solid phase toward the fluid phase and for the diffusion in the fluid phase, within the mesoporosity into the bio-ceramic particle, Galdi and Lamberti (26) proposed the following model (Eq. 3):

$$\begin{cases} \dfrac{\partial C}{\partial t} = \vec{\nabla} \cdot \left(D_L \vec{\nabla} C\right) - \dfrac{(1-\varepsilon)}{\varepsilon} \dfrac{\rho_s}{\rho_f} \dfrac{\partial Q}{\partial t} \dfrac{\partial Q}{\partial t} = -k_c (C^* - C) Q = K C^* \end{cases} \tag{3}$$

where $k_c$ is the drug molecule transfer coefficient from the pore surface to the fluid phase (per second): the greater its value, the smaller the resistance to the transport encountered by the drug. $C^*$ represents the drug concentration at solid–fluid interface (fluid side), in equilibrium with the solid-side concentration $Q^*$ (supposed as uniform on the whole internal channels' surface, i.e., $Q=Q^*$), according to the simple partition relation in which $K$ is the partition factor. The water molecule is very small in comparison with the drug molecule, so the diffusion of water within the pores is faster than the drug desorption and diffusion, at least of some order of magnitude. A largely faster phenomenon does not have any effect on the overall release kinetics, and thus, it can be neglected from the modeling point of view.

To be solved, the model requires the definition of appropriate initial and boundary conditions, the knowledge of the system's parameters (geometry, porosity $\varepsilon$=0.76, estimated on the basis of pore volume; solid density $\rho_s$= 2,600 mg $cm^{-3}$; fluid density $\rho_f$=1,000 mg $cm^{-3}$) and the determination of equilibrium and transport parameters. To simplify the problem and to reduce the number of model parameters, the partition coefficient can be assumed to be unity. Thus, so forth in this work, $K$ was taken as equal to 1. The matrix is initially loaded with a homogeneous drug concentration, $Q_0$; the fluid phase is initially pure ($C_0$=0). On the external surface of the particles, a *perfect sink* condition is assumed. Particles' dimensions, in absence of erosion and swelling phenomena, are constant. For each time, the overall drug mass contained into the matrix ($m_F$) can be calculated as the sum of the mass contained into the solid phase and the mass contained into the liquid, i.e., Eq. 4:

$$m_F(t) = \int_V \rho_s (1-\varepsilon) Q \mathrm{d}V + \int_V \rho_f \varepsilon C \mathrm{d}V \tag{4}$$

where $V$ is the particle volume. Therefore, the fractional release can be calculated as (Eq. 5):

$$R(t) = 1 - m_F(t)/m_{F0} \tag{5}$$

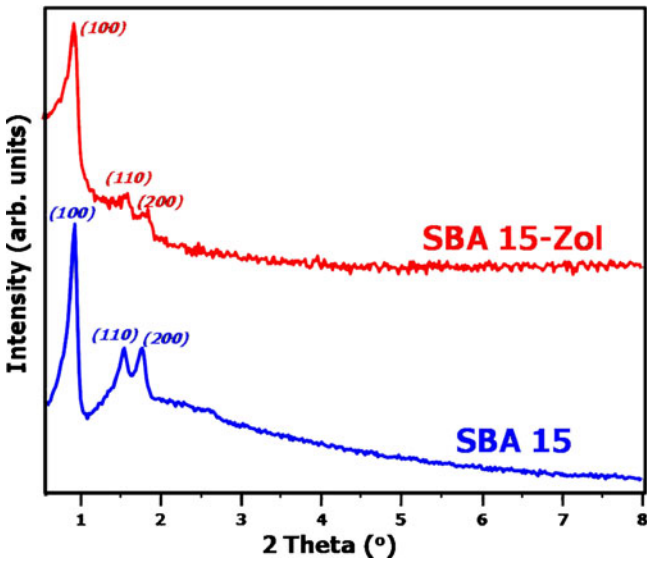


**Fig. 2.** Small-angle XRD patterns of SBA 15 before and after loading with zoledronate molecules

where $m_{F0}$ is the initial drug mass loaded in the device.

The model given by system (3) was successfully applied to the release of ibruprofen from MCM-41 bio-ceramic (26), a real case physically very close to the one considered here. The differences between these two systems, in term of drug molecular size, pore size, and matrix tortuosity, will be

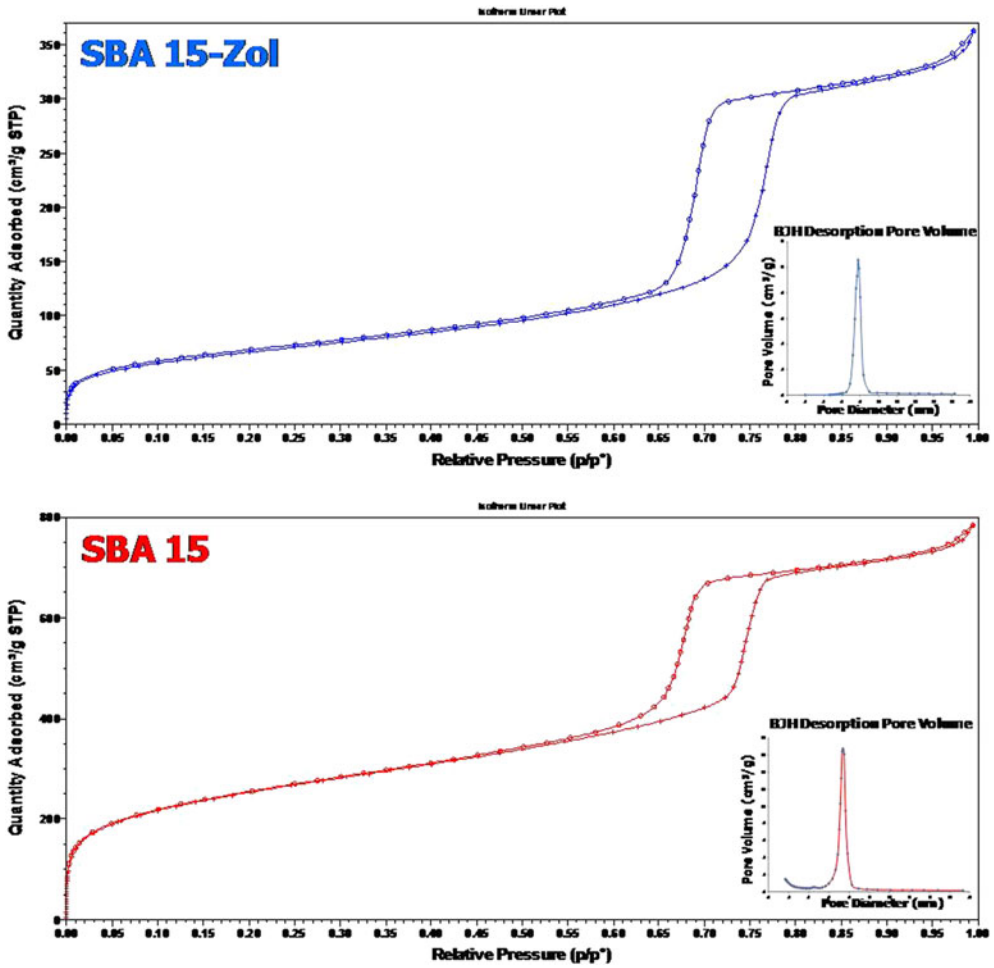


**Fig. 3.** $N_2$ adsorption isotherms of SBA 15 (*bottom*) and SBA 15 loaded with zoledronate (*top*). In both plots, as *insets* at the *right hand bottom corner*, it displayed the pore size distributions obtained using the BJH method

accounted for in the model parameters, in particular in the diffusivity coefficient $D_L$. Once the model was found able to describe the present case (zoledronate in SBA 15), the model proposed should be considered able to describe this class of systems (drug in bioceramics), which seems to be very important in the frame of drug delivery systems.

## RESULTS AND DISCUSSION

The ordered mesostructure of the produced SBA 15 material was confirmed by small-angle X-ray diffraction (Fig. 2). The XRD pattern of SBA 15 material was well resolved with a prominent maximum at 0.9° and two other weak maxima at 1.6° and 1.8° 2$\theta$. This maxima can be assigned to typical [100], [110], and [200] reflections of a two-dimensional hexagonal symmetry (*p6mm*). The hexagonal planar mesoporous structure was preserved after the zoledronate loading process, as can be observed in the XRD patterns, where similar diffraction maxima were observed (Fig. 2).

The $N_2$ adsorption isotherms of SBA 15 materials, both zoledronate loaded and unloaded, can be clearly attributed to a type IV in the BDDT classification (27), with the typical hysteresis loops of this type of mesoporous materials (Fig. 3). The shape of the hysteresis loops, with parallel adsorption and desorption branches, indicates cylindrical mesopores with very narrow pore size distributions. Attending to the obtained isotherm plots in Fig. 3, three different regions can be observed: (1) a linear region due to multilayer formation onto the external surface of the particles; (2) a step region due to capillary condensation within the mesopores; and (3) a linear region due to a multilayer adsorption in the mesopores. It should be highlighted that after loading the mesoporous matrices with zoledronate molecules, the mesostructured arrangement of the matrices survived the process, since the hysteresis loops present similar shape.

These types of $N_2$ adsorption analyses have been traditionally employed to confirm that the adsorbed molecules were into the inner part of the mesopores. This was assessed attending to the variation of some textural parameters, such as pore volume reduction and surface area reduction, as a consequence of drug molecules intake (Table I).

The available pore volume decreased after loading the matrix with zoledronate molecules, which is commonly used to verify that guest molecules is confined into the inner part of the mesopores. However, this is not a direct evidence of the presence of zoledronate into the pores. To do so, high-resolution Cs corrected STEM microscopy can be employed because it allows the qualitative determination of the presence of organic molecules into the inner area of mesoporous systems (28).

**Table I.** Textural Parameters of SBA 15 Before and After Zoledronate Loading

| Material | $S_{BET}$ ($m^2$/g) | $V_p$ ($cm^3$/g) | $V_{\mu p}$ ($cm^3$/g) | $D_p$ (nm) |
|---|---|---|---|---|
| SBA 15 | 903 | 1.21 | 0.046 | 7.4 |
| SBA 15-zol | 239 | 0.56 | 0.004 | 7.4 |

$S_{BET}$ is the surface area determined by using the BET method between the relative pressures ($P/P_0$) 0.05–0.25. $V_p$ and $V_{\mu p}$ are, respectively, the total pore volume and micropore volume obtained using the *t*-plot method. The total pore volume was estimated from the amount adsorbed at a relative pressure of 0.99. The average diameter of mesopores, $D_p$, was obtained from the maximum of a pore size distribution calculated using the Barrett–Joyner–Halenda (BJH) method applied to the desorption part of the isotherm (insets in Fig. 3)

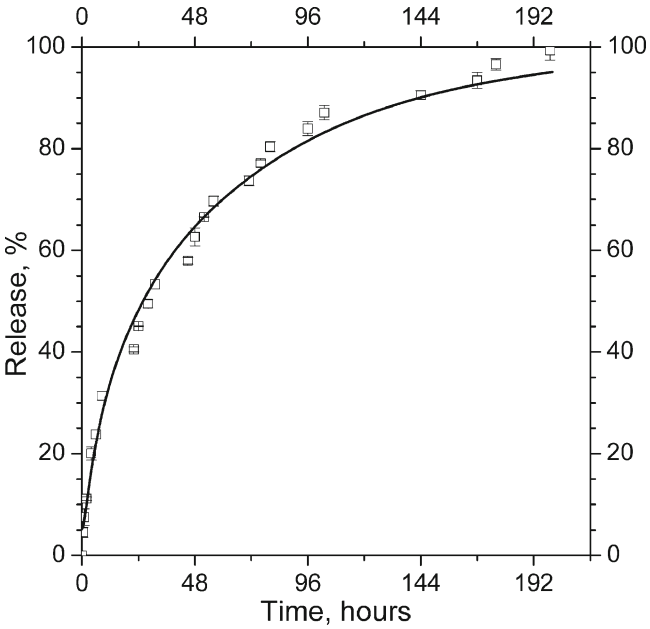


**Fig. 4.** Zoledronate release from SBA 15 materials. Symbols are the experimental data, and each point is the average over three independent measurements, the data being reported as the average value with its standard deviation as vertical error bars; the curve is the model calculation. The Pearson correlation coefficient between experimental data and model calculation is $R^2$=0.992

FTIR spectroscopy of SBA 15 materials (not shown) presented the typical vibration bands of siliceous materials: the asymmetric stretching Si–O–Si ($\nu_{SiOSi}$) vibration bands at ca. 1,085 $cm^{-1}$, the symmetric stretching Si–O ($\nu_{SiO}$) vibration bands at ca. 800 $cm^{-1}$, the Si–O–Si bending ($\delta_{SiOSi}$) vibration at ca. 470 $cm^{-1}$, and the stretching vibrations of Si–OH ($\nu_{SiOH}$) groups at ca. 960 $cm^{-1}$. In addition to those vibration bands, a broad band at ca. 3,400 $cm^{-1}$ was observed, which is characteristic of O–H stretching bands. They can be attributed to both Si–OH groups present on the surface of the matrix and/or some physisorbed water, which can be confirmed by the presence of HOH deformation band at ca. 1,620 $cm^{-1}$.

Unfortunately, the most characteristic vibration bands of bisphosphonates, stretching P=O (1,200–1,160 $cm^{-1}$), stretching P–OH (≈1,000 and ≈925 $cm^{-1}$), and deformation POH (ca. 1,080 $cm^{-1}$), were overlapped by SBA 15 vibration bands. However, the successful loading of zoledronate can be confirmed by the appearance of a small shoulder in the broad OH band commented above at ca. 2,900 and 2,800 $cm^{-1}$, which unequivocally represents the presence of C–H bonds (anti-symmetric and symmetric C–H stretching bands) and, consequently, confirms the presence of the alkyl chain from the drug. In addition to this, the presence of zoledronate within the matrix can be assured by the presence of the typical imidazole ring skeleton vibrations at ca. 1,500 $cm^{-1}$ and the asymmetric and symmetric ring C=C stretching vibrations at ca. 1,450 $cm^{-1}$.

The quantification of zoledronate loading was carried out using XRF, which is a method previously reported for the

quantification of bisphosphonates (18–20). Thus, attending to the total amount of elemental phosphorous contained after drug uptaking, SBA 15 materials loaded 120 mg of zoledronate per gram of mesoporous matrix.

The experimental zoledronate release profiles, shown in Fig. 4, denoted that in the tested conditions, there was a fast drug release at the beginning of the experiment (initial burst effect) followed by a more stationary release.

As it has been mentioned in above, the possibility of predicting the drug concentration within the body is one of the key aspects of pharmacology. In fact, the pharmacokinetic models try to predict the hematic concentration of drugs after the administration, and to do so, the *in vivo* experiments are the main source of information. However, due to their complications in terms of resource and time consuming, it is also possible to carry out *in vitro* experiments that provide modeling tools avoiding or minimizing the use of *in vivo* models (29,30). Thus, to model the release kinetics of this type of mesoporous matrices, it is necessary to take into account that the particles of loaded materials were shaped as tablets (disks). During the compaction process, small tunnels were produced between the particles. However, these micropores are considerably larger than the mesopores present within the bio-ceramics particles. Therefore, it is reasonable to assume that the drug encounters most of the resistance to its transportation within the mesopores into the particles and it was transported easily within the macro-pores between the particles. Thus, the pseudo-diffusion phenomena stated in the first of Eq. 3 and the pseudo-diffusion coefficient $D_L$ are both referred to the transport in the mesopores. In conclusion, the system (3) was written for spherical particles of a mean radius $R_S$=500 nm (the mean size expected for the particles), and the code was numerically solved.

The two parameters of the model were estimated on the basis of the same analysis performed on a similar system (MCM-41 bioceramics loaded with ibuprofen (26)). In particular for $k_c$, which represents a local transfer coefficient and is not correlated to the pore dimensions, the value of the mass transfer coefficient suggested by (26), equal to $1 \cdot 10^{-4}$ $s^{-1}$, was used. The pseudo-diffusivity $D_L$ was optimized by comparison with experimental data, and the value which gives the best agreement is $D_L = 1.65 \cdot 10^{-19}$ $m^2 s^{-1}$. The value of $D_L$ optimized is of the same order of magnitude of the values found for the same parameter on the MCM-41/ibuprofen system. In particular, the linear dependence discovered for the MCM-41 matrices between $D_L$ and pore's diameter returns, for a pore of 7.4 nm (pore size in the SBA-15 matrix), a $D_L$ value of about $4 \cdot 10^{-18}$ $m^2 s^{-1}$. The optimized value is about 20 times smaller, probably because of the larger molecular size of zoledronate compared with the molecular size of the ibuprofen or because of a higher tortuosity in the SBA-15 matrix with respect to the MCM-41 matrix due to the presence of micropores connecting the mesopores. The experimental data along with the model best fitting were reported in Fig. 4.

Summarizing, it should be noted that practically just one parameter has been optimized here, the diffusivity coefficient $D_L$, and its value is of the same order of magnitude found in the analysis of similar cases. Therefore, being the model in the present form *descriptive* of the phenomena observed, it could be used as a *predictive* tool for systems not too different from the present one, also guided by some role of thumb. For example, studying the release from a larger molecule from SBS-15 ceramics, the model will still hold in the calculation of release kinetics, maybe asking for a lower value of $D_L$.

## CONCLUSIONS

The release of a potent bone-resorption inhibitor, zoledronate, from ordered mesoporous materials, SBA 15, has been modeled. The obtained result for the prediction has been verified in an experimental model, which validates the modeling here presented. The significance of this work relies on the development of a very useful tool for the designing of implantable drug delivery systems allowing to predict the release kinetics of a biomolecule with anticipation. Consequently, in the near future, research capabilities would be more efficiently applied predicting release kinetics on advance, with the subsequent savings on time and resources.

## REFERENCES


1. Manzano M, Colilla M, Vallet-Regí M. Drug delivery from ordered mesoporous matrices. Expert Opin Drug Delivery. 2009;6(12):1383–400.
2. Izquierdo-Barba I, Ruiz-González L, Doadrio JC, González-Calbet JM, Vallet-Regí M. Tissue regeneration: a new property of mesoporous materials. Solid State Sci. 2005;7(8):983–9.
3. Vallet Regí M. Ordered mesoporous materials in the context of drug delivery systems and bone tissue engineering. Chem Eur J. 2006;12(23):5934–43.
4. Vallet Regí M. Nanostructured mesoporous silica matrices in nanomedicine. J Intern Med. 2010;267(1):22–43.
5. Manzano M, Vallet-Regí M. New developments in ordered mesoporous materials for drug delivery. J Mater Chem. 2010;20 (27):5593–604.
6. Colilla M, Manzano M, Vallet-Regí M. Recent advances in ceramic implants as drug delivery systems for biomedical applications. Int J Nanomed. 2008;3(4):403.
7. Hench LL, Wilson J. Surface-active biomaterials. Science. 1984;226:630–6.
8. Vallet-Regi MA, Ruiz-Gonzalez L, Izquierdo-Barba I, Gonzalez-Calbet JM. Revisiting silica based ordered mesoporous materials: medical applications. J Mater Chem. 2006;16(1):26–31. doi:10.1039/b509744d.
9. Rodan GA, Martin TJ. Therapeutic approaches to bone diseases. Science. 2000;289(5484):1508.
10. Russell R, Rogers M. Bisphosphonates: from the laboratory to the clinic and back again. Bone. 1999;25(1):97–106.
11. Nancollas G, Tang R, Phipps R, Henneman Z, Gulde S, Wu W, *et al.* Novel insights into actions of bisphosphonates on bone: differences in interactions with hydroxyapatite. Bone. 2006;38 (5):617–27.
12. Woo S, Hellstein J, Kalmar J. Narrative (corrected) review: bisphosphonates and osteonecrosis of the jaws (published correction appears in Ann Intern Med 2006; 145 [3]: 235). Ann Intern Med. 2006;144(10):753–61.
13. Nafea EH, El-Massik MA, El-Khordagui LK, Marei M, Khalafallah NM. Alendronate PLGA microspheres with high loading efficiency for dental applications. J Microencapsulation. 2007;24(6):525–38.
14. Baek JS, Kwon HH, Hwang JS, Sung HC, Lee JM, Shin SC, *et al.* Alendronate-loaded microparticles for improvement of intestinal cellular absorption. J Drug Target. 2011;19(1):37–48. doi:10.3109/10611861003667599.
15. Shi X, Wang Y, Ren L, Gong Y, Wang DA. Enhancing alendronate release from a novel PLGA/hydroxyapatite microspheric system for bone repairing applications. Pharm Res. 2009;26(2):422–30.

16. Josse S, Faucheux C, Soueidan A, Grimandi G, Massiot D, Alonso B, *et al*. Novel biomaterials for bisphosphonate delivery. Biomaterials. 2005;26(14):2073–80.
17. Peter B, Gauthier O, Laib S, Bujoli B, Guicheux J, Janvier P, *et al*. Local delivery of bisphosphonate from coated orthopedic implants increases implants mechanical stability in osteoporotic rats. J Biomed Mater Res Part A. 2006;76A(1):133–43. doi:10.1002/jbm.a.30456.
18. Balas F, Manzano M, Horcajada P, Vallet-Regí M. Confinement and controlled release of bisphosphonates on ordered mesoporous silica-based materials. J Am Chem Soc. 2006;128(25):8116–7.
19. Nieto A, Balas F, Colilla M, Manzano M, Vallet-Regí M. Functionalization degree of SBA-15 as key factor to modulate sodium alendronate dosage. Microporous Mesoporous Mater. 2008;116(1–3):4–13.
20. Colilla M, Manzano M, Izquierdo-Barba I, Vallet-Regi M, Boissiere C, Sanchez C. Advanced drug delivery vectors with tailored surface properties made of mesoporous binary oxides submicronic spheres. Chem Mater. 2010;22(5):1821–30. doi:10.1021/cm9033484.
21. Colilla M, Izquierdo-Barba I, Vallet-Regi M. Phosphorus-containing SBA-15 materials as bisphosphonate carriers for osteoporosis treatment. Microporous Mesoporous Mater. 2010;135(1–3):51–9.
22. Chirico S, Dalmoro A, Lamberti G, Russo G, Titomanlio G. Analysis and modeling of swelling and erosion behavior for pure HPMC tablet. J Controlled Release. 2007;122(2):181–8. doi:10.1016/j.jconrel.2007.07.001.
23. Zhao DY, Feng JL, Huo QS, Melosh N, Fredrickson GH, Chmelka BF, *et al*. Triblock copolymer syntheses of mesoporous silica with periodic 50 to 300 angstrom pores. Science. 1998;279 (5350):548–52.
24. Lapidus L, Pinder GF. Numerical solution of partial differential equations in science and engineering. New York: Wiley-Interscience; 1982.
25. COMSOL. Multiphysics User's Guide: Comsol AB; 1994–2007.
26. Galdi I, Lamberti G. Drug release from matrix systems. Analysis by finite element methods heat and mass transfer. 2011. doi:10.1007/s00231-011-0900-y.
27. Sing K, Gregg S. Adsorption, surface area and porosity. London: Academic Press; 1982.
28. Vallet-Regi M, Manzano M, Gonzalez-Calbet JM, Okunishi E. Evidence of drug confinement into silica mesoporous matrices by STEM spherical aberration corrected microscopy. Chem Commun. 2010;46(17):2956–8. doi:10.1039/c000806k.
29. Di Muria M, Lamberti G, Titomanlio G. Modeling the pharmacokinetics of extended release pharmaceutical systems. Heat Mass Transfer. 2009;45(5):579–89. doi:10.1007/s00231-008-0456-7.
30. Di Muria M, Lamberti G, Titomanlio G. Physiologically based pharmacokinetics: a simple, all purpose model. Ind Eng Chem Res. 2010;49(6):2969–78.